Chemical chaperone ameliorates pathological protein aggregation in plectin-deficient muscle

Lilli Winter,[1] Ilona Staszewska,[1] Eva Mihailovska,[1] Irmgard Fischer,[1] Wolfgang H. Goldmann,[2] Rolf Schröder,[3] and Gerhard Wiche[1]

[1]Department of Biochemistry and Cell Biology, Max F. Perutz Laboratories, University of Vienna, Vienna, Austria. [2]Department of Physics, Center for Medical Physics and Technology, Friedrich-Alexander-University Erlangen-Nuremberg, Erlangen, Germany. [3]Institute of Neuropathology, University Hospital Erlangen, Erlangen, Germany.

The ubiquitously expressed multifunctional cytolinker protein plectin is essential for muscle fiber integrity and myofiber cytoarchitecture. Patients suffering from plectinopathy-associated epidermolysis bullosa simplex with muscular dystrophy (EBS-MD) and mice lacking plectin in skeletal muscle display pathological desmin-positive protein aggregation and misalignment of Z-disks, which are hallmarks of myofibrillar myopathies (MFMs). Here, we developed immortalized murine myoblast cell lines to examine the pathogenesis of plectinopathies at the molecular and single cell level. Plectin-deficient myotubes, derived from myoblasts, were fully functional and mirrored the pathological features of EBS-MD myofibers, including the presence of desmin-positive protein aggregates and a concurrent disarrangement of the myofibrillar apparatus. Using this cell model, we demonstrated that plectin deficiency leads to increased intermediate filament network and sarcomere dynamics, marked upregulation of HSPs, and reduced myotube resilience following mechanical stretch. Currently, no specific therapy or treatment is available to improve plectin-related or other forms of MFMs; therefore, we assessed the therapeutic potential of chemical chaperones to relieve plectinopathies. Treatment with 4-phenylbutyrate resulted in remarkable amelioration of the pathological phenotypes in plectin-deficient myotubes as well as in plectin-deficient mice. Together, these data demonstrate the biological relevance of the MFM cell model and suggest that this model has potential use for the development of therapeutic approaches for EBS-MD.

Introduction

Protein aggregation is the characteristic pathomorphological hallmark of major neurodegenerative disorders such as Alzheimer's and Parkinson's disease, various forms of dementia, and amyotrophic lateral sclerosis. In analogy to this group of central nervous system disorders, pathological protein aggregation also plays an important role in a variety of human myopathies. Myofibrillar myopathies (MFMs) are an expanding group of clinically and genetically heterogeneous muscle diseases characterized by pathological desmin-positive protein aggregates, myofibrillar degeneration, and mitochondrial abnormalities. MFMs are caused by mutations in genes encoding a variety of sarcomeric and extrasarcomeric proteins, including desmin, αB-crystallin, filamin C, VCP, myotilin, ZASP, FHL1, BAG3, DNAJB6, and plectin (1–3). To date, no specific therapy or even ameliorating treatment is available for this numerically significant cohort of hereditary myopathies.

Plectin, a giant (>500-kDa) multifunctional cytolinker protein of universal occurrence, plays a crucial role in stabilizing and orchestrating intermediate filament (IF) networks in cells (4, 5). Besides interacting with and affecting the dynamics of cytoskeletal filament systems (IFs, actin filaments, microtubules), plectin serves as a scaffolding platform for signaling molecules, thereby expanding its cytolinker function. Plectin's diversity is in part due to an unusually high number of alternatively spliced first exons, which give rise to distinct plectin isoforms that just differ in their very N-terminal sequences (6). These variable sequences determine the cellular targeting of the isoforms, thus enabling them to fulfill distinct functions in different cell types and tissues (3–5). The 4 major plectin isoforms expressed in skeletal muscle, plectin 1d (P1d), P1f, P1b, and P1, are crucial for myofibers by specifically targeting and anchoring desmin IFs to Z-disks, costameres, mitochondria, and the nuclear/ER membrane system, respectively (7, 8). In the absence of plectin, skeletal muscle fibers lose their structural integrity, as observed in patients suffering from plectinopathies and plectin-deficient mice. The most common disease caused by mutations in the human plectin gene (*PLEC*) is epidermolysis bullosa simplex with muscular dystrophy (EBS-MD), a rare autosomal skin blistering disorder associated with late-onset muscular dystrophy. In addition to EBS-MD, plectin mutations have been shown to cause EBS-MD with a myasthenic syndrome, EBS with pyloric atresia, limb-girdle muscular dystrophy type Q2, and EBS-Ogna (3).

Plectin-deficient (null) mice display multiple structural abnormalities reminiscent of minicore myopathies in skeletal muscle and disintegration of intercalated disks in heart (9). However, as an animal model for investigating the type of late-onset muscular dystrophy that is characteristic of plectinopathies, such mice are of limited use as they die within 2 to 3 days after birth. This problem has been overcome by generating conditional plectin knockout mice (MCK-Cre/cKO mice) with plectin deficiency restricted to skeletal muscle (8). Showing progressive degenerative alterations in striated muscle, including desmin IF network collapse, pathological protein aggregation, misalignment of Z-disks, detachment of the contractile apparatus from the sarcolemma, changes in costameric cytoarchitecture, and disruption of the mitochondrial network combined with dysfunction and loss of mitochondria (8), MCK-Cre/cKO mice closely mimic the pathology of patients suffering from plectinopathies (3, 8).

Conflict of interest: The authors have declared that no conflict of interest exists.
Citation for this article: *J Clin Invest.* 2014;124(3):1144–1157. doi:10.1172/JCI71919.

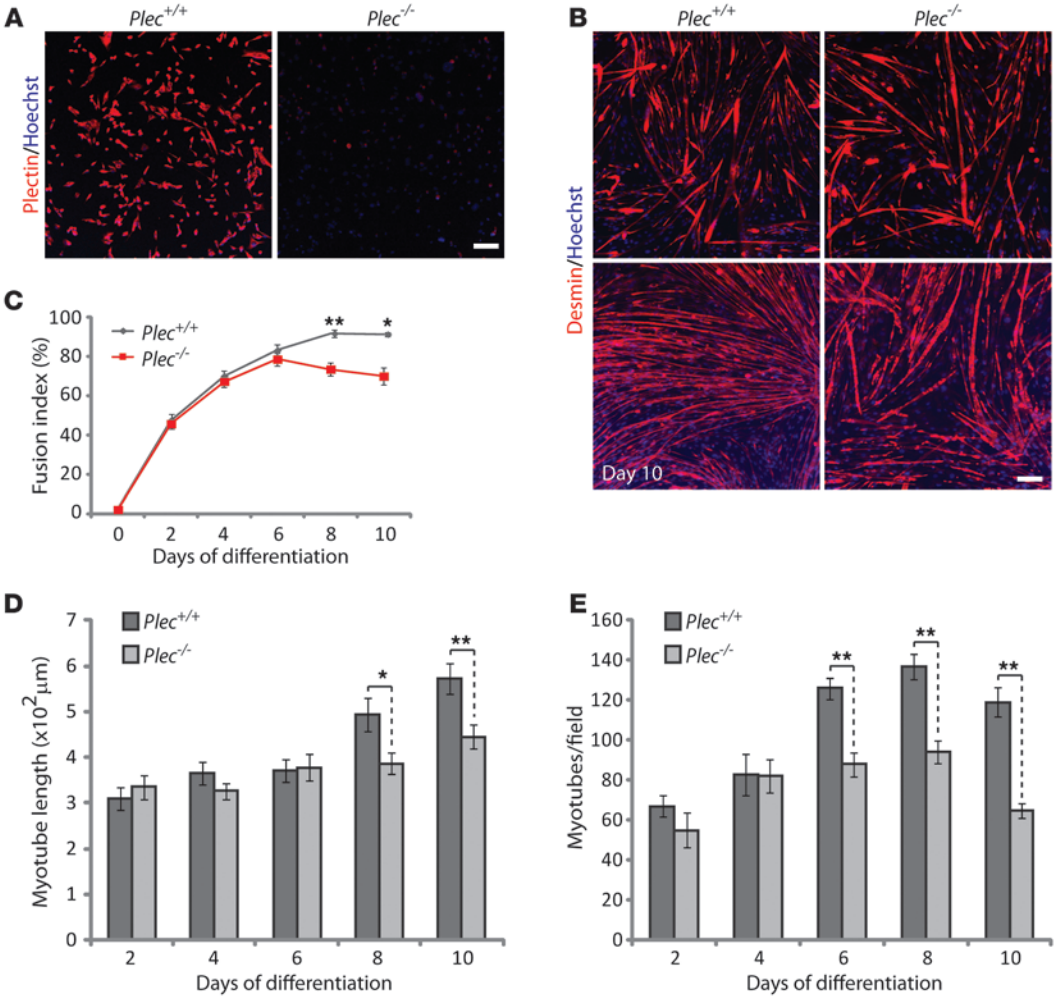

Figure 1

Plec$^{+/+}$ and *Plec*$^{-/-}$ myoblasts differentiate and form multinucleated myotubes in culture. (**A**) Immunostaining of plectin-positive (*Plec*$^{+/+}$) and plectin-deficient (*Plec*$^{-/-}$) myoblasts using pan-plectin antibodies and visualization of nuclei (Hoechst). (**B**) Myotubes differentiated for the time indicated were subjected to immunostaining (desmin) and staining with Hoechst dye. Scale bars: 100 µm (**A** and **B**). (**C**) Fusion indices (ratio of differentiated myotubes containing 2 or more nuclei to the total number of desmin-positive cells). (**D**) Length of myotubes. (**E**) Absolute number of myotubes per randomly chosen microscopic field. Data shown in **C**–**E** represent mean ± SEM, 3 experiments each. **P* < 0.05, ***P* < 0.01, unpaired Student's *t* test.

For studying the pathogenesis of plectinopathies and other MFMs at the molecular and single cell level, ex vivo cell cultures derived from patients, or from transgenic mouse lines that mimic the pathologic features of MFM myofibers, could be highly beneficial. Such systems would open the door to biochemical and/or cell biological analyses, including live imaging techniques, which are barely applicable in tissue. Moreover, they have a great potential in serving as screening and test systems for the development of novel treatment concepts. Primary cell cultures, directly derived from live skeletal muscle tissue, closely mimic the in vivo state but often represent heterogeneous mixtures of myoblasts and fibroblasts. Usually, fibroblasts double more rapidly and after several days become the predominant cell type. Moreover, primary cells display limited mitotic capacity in vitro, requiring repeated isolations, thus increasing interexperimental variability. We reasoned that such drawbacks could probably be avoided if myoblasts retaining a high myogenic potential could be immortalized and used instead of primary cultures. As spontaneously immortalized cell lines, such as commonly used C2C12 cells, show only a limited myogenic potential (10), we directly established a cell line of immortalized myoblasts from plectin-deficient muscle tissue of mice that additionally were deficient in p53. We show here that myoblasts of this type can differentiate into fully functional (contractile) myotubes that closely mimic the pathology of patients suffering from plectinopathies, including desmin aggregate formation and sarcomeric alterations, the hallmarks of MFMs. Using this new cell model, we could demonstrate that plectin deficiency leads to an increase in IF network and sarcomere dynamics, lower resilience toward mechanical stretch, and a marked upregulation of heat shock proteins (HSPs). In assessing potential treatment options for patients, we found the chemical chaperon 4-phenylbutyrate (4-PBA) to ameliorate some of the pathological phenotypes not only in these cells, but also in the corresponding plectin-deficient mouse line.

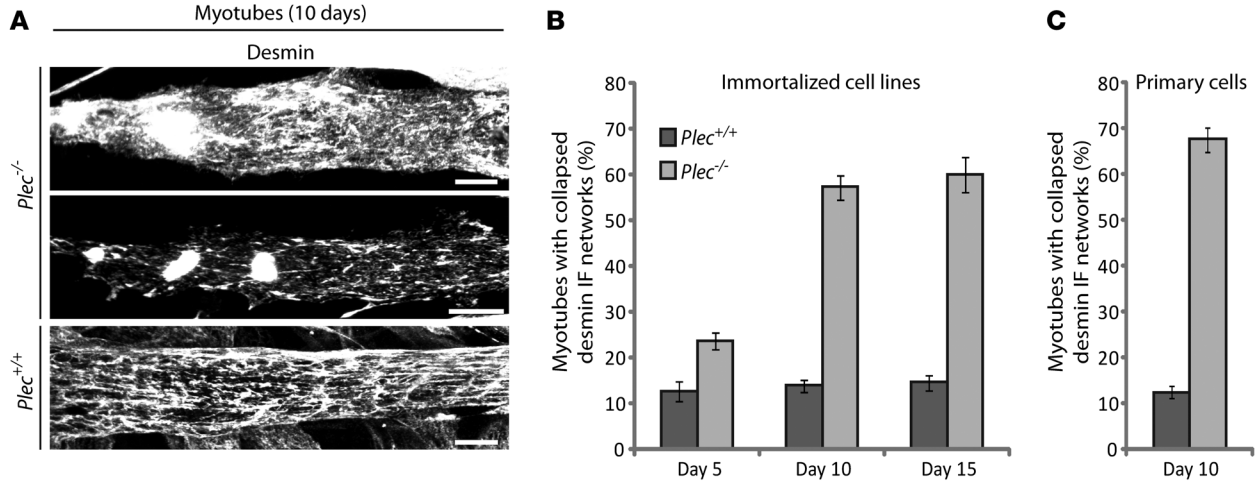

Figure 2
Spontaneous collapse of desmin IF networks upon plectin deficiency. (**A**) Desmin-specific immunostaining of *Plec*$^{+/+}$ and *Plec*$^{-/-}$ myotubes (differentiated for 10 days). *Plec*$^{-/-}$ myotubes with partially collapsed networks and massive desmin aggregates are shown in top and middle images, respectively. Scale bars: 10 μm. (**B**) Statistical analysis of desmin aggregate formation in *Plec*$^{+/+}$ and *Plec*$^{-/-}$ myotubes differentiated for 5 (*Plec*$^{+/+}$, $n = 436$ myotubes; *Plec*$^{-/-}$, $n = 383$ myotubes), 10 (*Plec*$^{+/+}$, $n = 363$ myotubes; *Plec*$^{-/-}$, $n = 356$ myotubes), or 15 (*Plec*$^{+/+}$, $n = 420$ myotubes; *Plec*$^{-/-}$, $n = 278$ myotubes) days. Mean ± SEM, 4 experiments. (**C**) Statistical evaluation of desmin aggregate formation in primary myotubes differentiated for 10 days (*Plec*$^{+/+}$, $n = 87$ myotubes; *Plec*$^{-/-}$, $n = 164$ myotubes). Mean ± SEM, 3 experiments.

Results

Plectin-deficient myoblasts differentiate and form contractile multinucleated myotubes in vitro. The strategy pursued in this study for isolating immortalized myoblasts was based on mouse lines (9) that had been crossed into a *p53*$^{-/-}$ background (11). Cultures of immortalized plectin-deficient (*Plec*$^{-/-}$) and plectin-positive (*Plec*$^{+/+}$) myoblasts were isolated and purified from fibroblasts to a homogeneity of >90% of desmin-positive cells (L. Winter, unpublished observations). *Plec*$^{-/-}$ myoblasts (Figure 1A) isolated in this way resembled *Plec*$^{+/+}$ cells in morphology and expressed desmin at comparative levels (Figure 1B). To evaluate the potential of *Plec*$^{-/-}$ myoblasts to undergo differentiation, their capacity to form multinucleated myotubes upon mitogen withdrawal was monitored. After 48 hours, *Plec*$^{-/-}$ myoblasts, similar to *Plec*$^{+/+}$ myoblasts, displayed the typical elongated and multinucleated morphology of differentiated myotubes (Figure 1B).

Moreover, *Plec*$^{-/-}$ myotubes, like their counterparts, showed spontaneous contractions after 1 week of differentiation (Supplemental Videos 1 and 2; supplemental material available online with this article; doi:10.1172/JCI71919DS1). When monitored over a 10-day period, similar fusion indices were observed within the first 6 days, with 83% of *Plec*$^{+/+}$ cells and 79% of *Plec*$^{-/-}$ cells being differentiated at day 6. Thereafter, fusion indices of *Plec*$^{-/-}$ myotubes declined to 70%, whereas those of *Plec*$^{+/+}$ myotubes increased to 91% (Figure 1C). Similarly, the average length of myotubes and the total number of myotubes per randomly chosen microscopic field was comparable in both cultures within the first days of differentiation (Figure 1, D and E). Interestingly, however, the number of *Plec*$^{-/-}$ myotubes remaining attached to the culture dishes after 6 days of differentiation was decreased compared with *Plec*$^{+/+}$ myotubes (Figure 1E), and the average length of *Plec*$^{-/-}$ myotubes remained constant while *Plec*$^{+/+}$ cells were still growing (Figure 1D); no differences were observed in the diameter of differentiated *Plec*$^{+/+}$ and *Plec*$^{-/-}$ myotubes (L. Winter, unpublished observations). These observations indicated that, while the initial capacity of *Plec*$^{-/-}$ myoblasts to form myotubes was unimpaired, the myotubes formed displayed diminished survival rates compared with those of *Plec*$^{+/+}$ cells.

Spontaneous desmin IF network collapse in plectin-deficient myotubes. In skeletal muscle tissue, plectin was shown to directly bind to desmin and to orchestrate desmin IF network architecture throughout the cytoplasm, at the sarcolemma, and at the levels of Z-disks, thereby preserving the functional integrity of muscle fibers (8). Similarly, in differentiated *Plec*$^{+/+}$ myotubes, plectin networks colocalized with desmin IFs and, beyond that, formed structures that clearly associated with α-actinin–positive Z-disks in a cross-striated staining pattern (Supplemental Figure 1). After differentiation for 20 days, part of the desmin networks also appeared to be associated with Z-disks. A comparison with teased myofibers generated from adult extensor digitorum longus muscle (EDL) revealed that differentiated myotubes closely resembled mature intact fibers (Supplemental Figure 1).

In plectin-deficent muscle fibers, desmin IFs were no longer found to be organized as networks; instead, desmin-positive aggregates became apparent throughout the sarcoplasm and in subsarcolemmal regions (8). Similarly, after differentiation of *Plec*$^{-/-}$ myotubes for 10 days, a large proportion of myotubes showed desmin-positive aggregates at a level ranging from partially collapsed networks in certain areas and intact networks in other areas of the same fiber (Figure 2A, top image) to fibers with massive desmin aggregates and hardly any IF network structures left (Figure 2A, middle image); aggregates of the latter category were never observed in *Plec*$^{+/+}$ (control) myotubes (Figure 2A, bottom image). To monitor the formation of aggregates and the proportion of affected cells in the course of differentiation, *Plec*$^{+/+}$ and *Plec*$^{-/-}$ myotubes were analyzed at days 5, 10, and 15 of differentiation. At as early as 5 days, collapsed desmin networks were observed in 24% of *Plec*$^{-/-}$ myotubes, compared with 13% in *Plec*$^{+/+}$

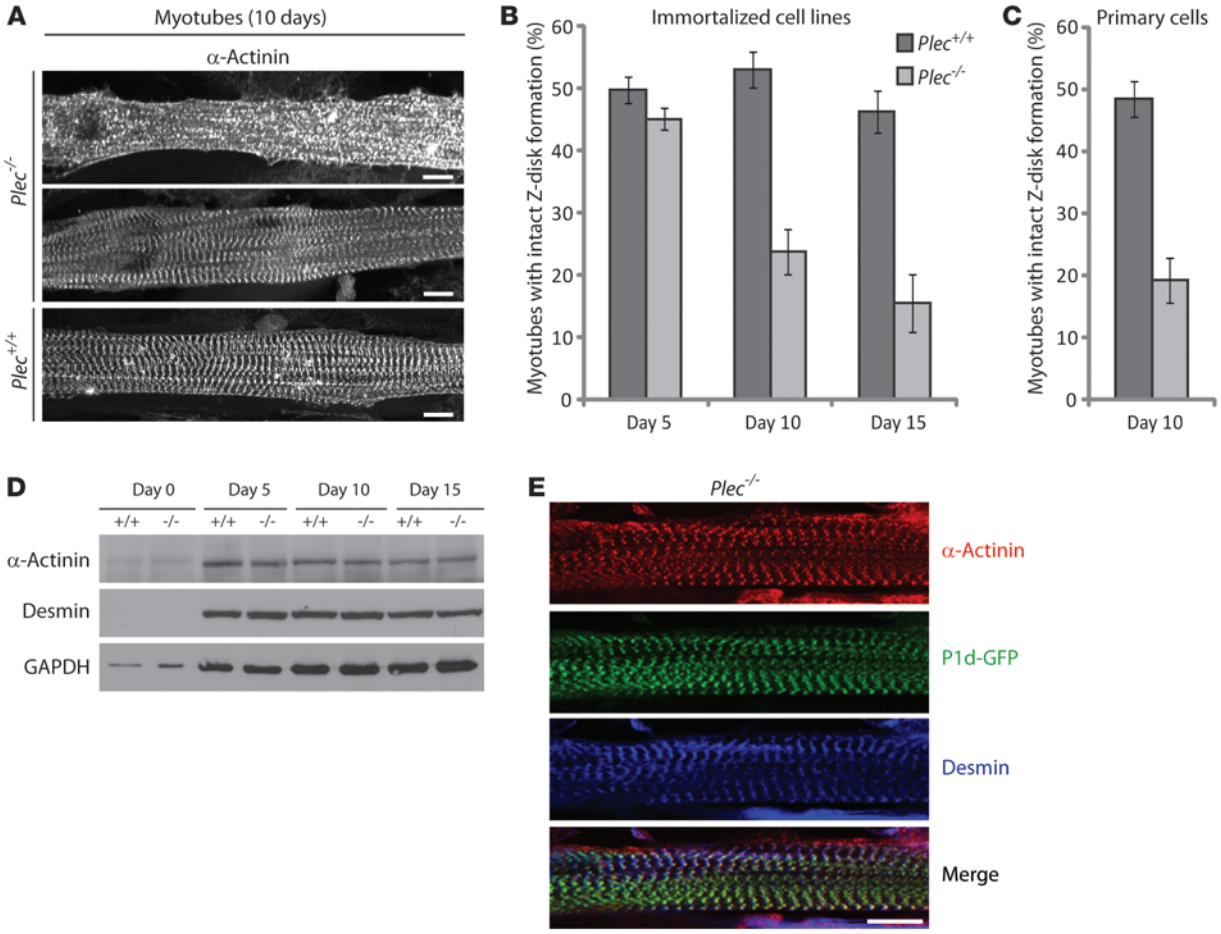

Figure 3

Z-disk formation in differentiated myotubes. (**A**) Z-disk formation was analyzed in *Plec*$^{+/+}$ and *Plec*$^{-/-}$ myotubes (differentiated for 10 days) by immunolabeling using antibodies to α-actinin. *Plec*$^{-/-}$ myotubes displaying dissolution of sarcomeric structures (top image) or intact Z-striations (middle image) are shown. Scale bars: 10 μm. (**B**) Statistical evaluation of intact sarcomeric structures observed in myotubes differentiated for 5 (*Plec*$^{+/+}$, $n = 426$ myotubes; *Plec*$^{-/-}$, $n = 279$ myotubes), 10 (*Plec*$^{+/+}$, $n = 330$ myotubes; *Plec*$^{-/-}$, $n = 384$ myotubes), or 15 (*Plec*$^{+/+}$, $n = 353$ myotubes; *Plec*$^{-/-}$, $n = 274$ myotubes) days. Mean ± SEM, 4 experiments. (**C**) Statistical evaluation of intact sarcomere formation in primary myotubes differentiated for 10 days (*Plec*$^{+/+}$, $n = 87$ myotubes; *Plec*$^{-/-}$, $n = 164$ myotubes). Mean ± SEM, 3 experiments. (**D**) Immunoblotting of cell lysates prepared from *Plec*$^{+/+}$ or *Plec*$^{-/-}$ myoblasts that were either undifferentiated (day 0) or differentiated for 5, 10, or 15 days. Antibodies used for detection are indicated. GAPDH was used as loading control. (**E**) *Plec*$^{-/-}$ myotubes expressing P1d-EGFP were differentiated for 10 days and immunolabeled using antibodies to desmin and α-actinin. Note that Z-disk formation was restored and desmin was recruited to sarcomeres. Scale bar: 10 μm.

cells. At days 10 and 15 after fusion, the proportion of affected fibers in plectin-deficient cultures increased to 57% and 60%, respectively, while the amount of fibers harboring collapsed IF networks in *Plec*$^{+/+}$ cultures stayed more or less constant (14% at day 10, 15% at day 15; Figure 2B).

Being derived from *p53*$^{-/-}$ mice, and thus lacking p53 in addition to plectin, our immortalized cell lines represented a double-knockout system. To rule out that p53 deficiency was causing, or contributing to, elevated desmin IF aggregation, similar experiments were performed with primary myoblast cultures derived from plectin-deficient mice and their wild-type littermates that were p53-positive (*p53*$^{+/+}$). As shown in Figure 2C, the percentage of primary plectin-deficient myotubes displaying collapsed IF networks after differentiation for 10 days was even higher (68%) than that observed in the case of their immortalized counterparts (compare with Figure 2B).

Isoform-specific rescue of sarcomere integrity in plectin-deficient myotubes by P1d. To assess whether myofibrillar structures were affected by plectin deficiency, sarcomere formation in *Plec*$^{-/-}$ and *Plec*$^{+/+}$ myotubes differentiated for 10 days was monitored by immunofluorescence microscopy using antibodies to Z-disk–associated α-actinin. While sarcomeric structures with a fully developed cross-striated staining pattern were visualized in both cell lines (Figure 3A, middle and bottom images), a substantial proportion of *Plec*$^{-/-}$ myotubes manifested with disorganized myofibrillar structures, displaying disoriented rather than continuous transverse α-actinin–specific staining patterns (Figure 3A, top image).

When immortalized cell lines were differentiated for 5, 10, or 15 days, 50% of *Plec*$^{+/+}$ myotubes were found to display well-organized sarcomeric structures at day 5, and the proportion of cells with clearly outlined sarcomeres was rather stable until day 15 (Figure 3B). Similarly, 45% of *Plec*$^{-/-}$ myotubes displayed sarcomeric struc-

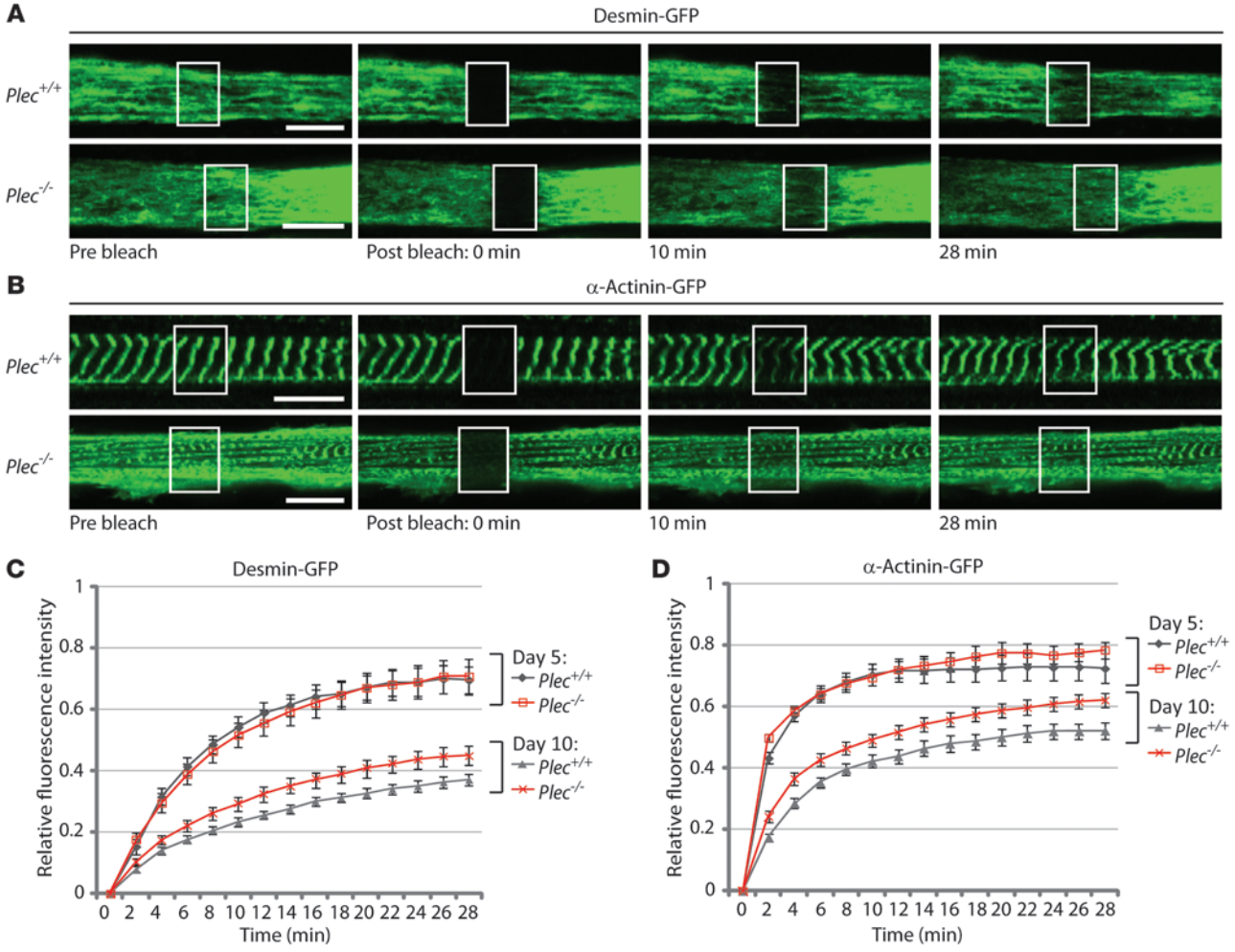

Figure 4

Dynamics of GFP-labeled desmin and α-actinin in differentiated myotubes monitored by FRAP analyses. (**A** and **B**) Representative (**A**) desmin-GFP– or (**B**) α-actinin–GFP–expressing *Plec*$^{+/+}$ and *Plec*$^{-/-}$ myotubes (differentiation for 10 days) are shown prior to photobleaching, immediately after photobleaching, and after 10 and 28 minutes of recovery. Bleached areas are indicated by boxes. Scale bars: 10 μm. (**C**) FRAP analyses of desmin-GFP in *Plec*$^{+/+}$ and *Plec*$^{-/-}$ myotubes differentiated for 5 or 10 days. Mean ± SEM, 2 experiments (5 days of differentiation: *Plec*$^{+/+}$, $n = 25$ analyzed ROIs; *Plec*$^{-/-}$, $n = 21$ analyzed ROIs; 10 days of differentiation: *Plec*$^{+/+}$, $n = 54$ analyzed ROIs; *Plec*$^{-/-}$, $n = 55$ analyzed ROIs). (**D**) FRAP analysis of α-actinin–GFP under conditions similar to those in **C**. Mean ± SEM, 2 experiments (5 days of differentiation: *Plec*$^{+/+}$, $n = 25$ analyzed ROIs; *Plec*$^{-/-}$, $n = 26$ analyzed ROIs; 10 days of differentiation: *Plec*$^{+/+}$, $n = 38$ analyzed ROIs; *Plec*$^{-/-}$, $n = 45$ analyzed ROIs).

tures at day 5. At later time points, however, plectin-deficient myotubes showed drastic alterations of sarcomeric organization. In fact, only 24% of *Plec*$^{-/-}$ myotubes displayed regular α-actinin–positive striations at day 10, compared with 53% in *Plec*$^{+/+}$ cultures. At day 15 after fusion, 85% of *Plec*$^{-/-}$ myotubes myofibrillar structures were grossly disorganized, while 46% of *Plec*$^{+/+}$ myotubes still contained organized sarcomeres (Figure 3B). Similar results were obtained when primary myoblast cultures were analyzed, confirming the observed phenotype irrespective of p53 deficiency (Figure 3C).

In skeletal muscle tissue lysates, total desmin protein levels had been found to be reduced in MCK-Cre/cKO mice compared with those in wild-type mice, while α-actinin levels were similar in both cases (8). In contrast, when lysates of *Plec*$^{+/+}$ and *Plec*$^{-/-}$ myoblast cell lines, differentiated for 5, 10, or 15 days, were subjected to immunoblotting analysis, we did not observe differences in desmin or α-actinin expression levels in any of the cases (Figure 3D).

To test the potential of the Z-disk–associated plectin isoform P1d to revert the phenotypes of *Plec*$^{-/-}$ myotubes, expression plasmids, encoding full-length P1d (C-terminally fused to EGFP), were transiently transfected into *Plec*$^{-/-}$ myoblasts. After differentiation for 10 days, myotubes were subjected to immunofluorescence microscopy using antibodies to α-actinin and desmin. As shown in Figure 3E, P1d was found to be fully capable of restoring sarcomere formation in *Plec*$^{-/-}$ cells (for a quantitative analysis of Z-disk restoration by P1d in comparison to other plectin isoforms see Supplemental Figure 2D). Moreover, it effected the recruitment of IF networks to the Z-disks, as indicated by the cross-striated staining pattern of desmin (Figure 3E). In contrast, the forced expression of other isoforms, such as P1, P1b, and P1f, did not restore sarcomeric structures (Supplemental Figure 2), clearly indicating that plectin's rescue potential was specific for P1d, the only isoform that is exclusively associated with Z-disks.

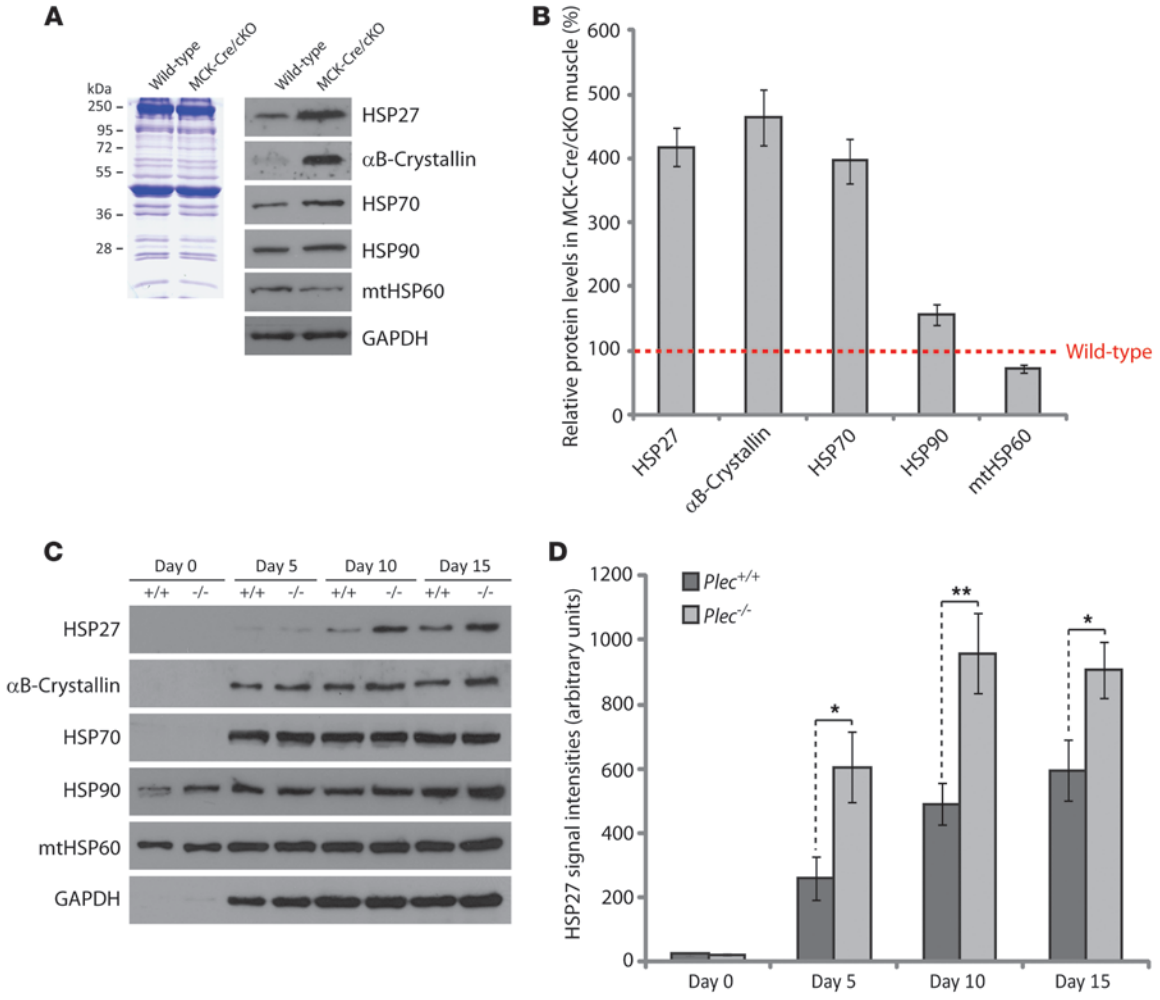

Figure 5

Expression profiles of chaperones in plectin-deficient muscle fibers and differentiated myotubes. (**A**) Equal amounts of wild-type and plectin-deficient (MCK-Cre/cKO) gastrocnemius muscle lysates were subjected to immunoblotting analysis using antibodies as indicated. GAPDH was used as loading control. (**B**) Signal intensities were densitometrically measured and normalized to total protein content. Mean ± SEM, 3 experiments. (**C**) *Plec*$^{+/+}$ and *Plec*$^{-/-}$ myoblasts were differentiated for the time periods indicated, and cell lysates prepared at days 0, 5, 10, and 15 were analyzed by immunoblotting as in **A**. (**D**) Signal intensities of HSP27 protein bands shown in **C** were measured and normalized as in **B**. Mean ± SEM, 3 experiments. *$P < 0.05$, **$P < 0.01$, unpaired Student's *t* test.

Apart from desmin protein aggregation and Z-disk misalignment, *Plec*$^{-/-}$ myoblasts showed a third major MFM hallmark, i.e., mitochondrial abnormalities (see Supplemental Figure 3 and Supplemental Methods).

Plectin deficiency leads to increased IF network and sarcomere dynamics. When myoblasts fuse to form multinucleated myotubes, they develop desmin filament networks and build up sarcomeres. As plectin deficiency leads to alterations in the cytoarchitecture of myofibers, we wondered whether it had an impact on the dynamic assembly of desmin networks and Z-disk–associated α-actinin–containing structures. To assess this, we transfected *Plec*$^{+/+}$ and *Plec*$^{-/-}$ myoblasts with EGFP coupled to desmin (Figure 4A) or α-actinin (Figure 4B) and analyzed protein dynamics inside living myotubes by fluorescence recovery after photobleaching (FRAP). After 5 days of differentiation, we found both proteins to be in a highly dynamic state, with 70% and 75% of desmin and α-actinin molecules, respectively, contributing to the mobile fraction in *Plec*$^{+/+}$ as well as *Plec*$^{-/-}$ myotubes. Reaching a plateau level after only approximately 10 minutes, the overall recovery rate of α-actinin was faster compared with that of desmin (~30 minutes); however, significant differences in recovery rates were not observed for either protein in *Plec*$^{+/+}$ and *Plec*$^{-/-}$ myotubes at this time point of differentiation (Figure 4, C and D). Upon further differentiation and maturation of cytoskeletal and sarcomeric structures, protein mobilities decreased. Interestingly, while in *Plec*$^{+/+}$ myotubes after 10 days only 37% of desmin molecules exchanged within 28 minutes; in their *Plec*$^{-/-}$ counterparts, desmin fluorescence recovered to 45% of the initial intensity within the same period. This indicated that the mobility of desmin molecules was increased in *Plec*$^{-/-}$ cells compared with that in *Plec*$^{+/+}$ cells (Figure 4C). Similarly, when sarcomeric structures were analyzed in *Plec*$^{+/+}$ myotubes after 10 days of differentiation, we found α-actinin fluorescence to recover to 52% of the initial intensity within 28 minutes, whereas in plectin-deficient specimens it reached 62% (Figure 4D). The conclusion

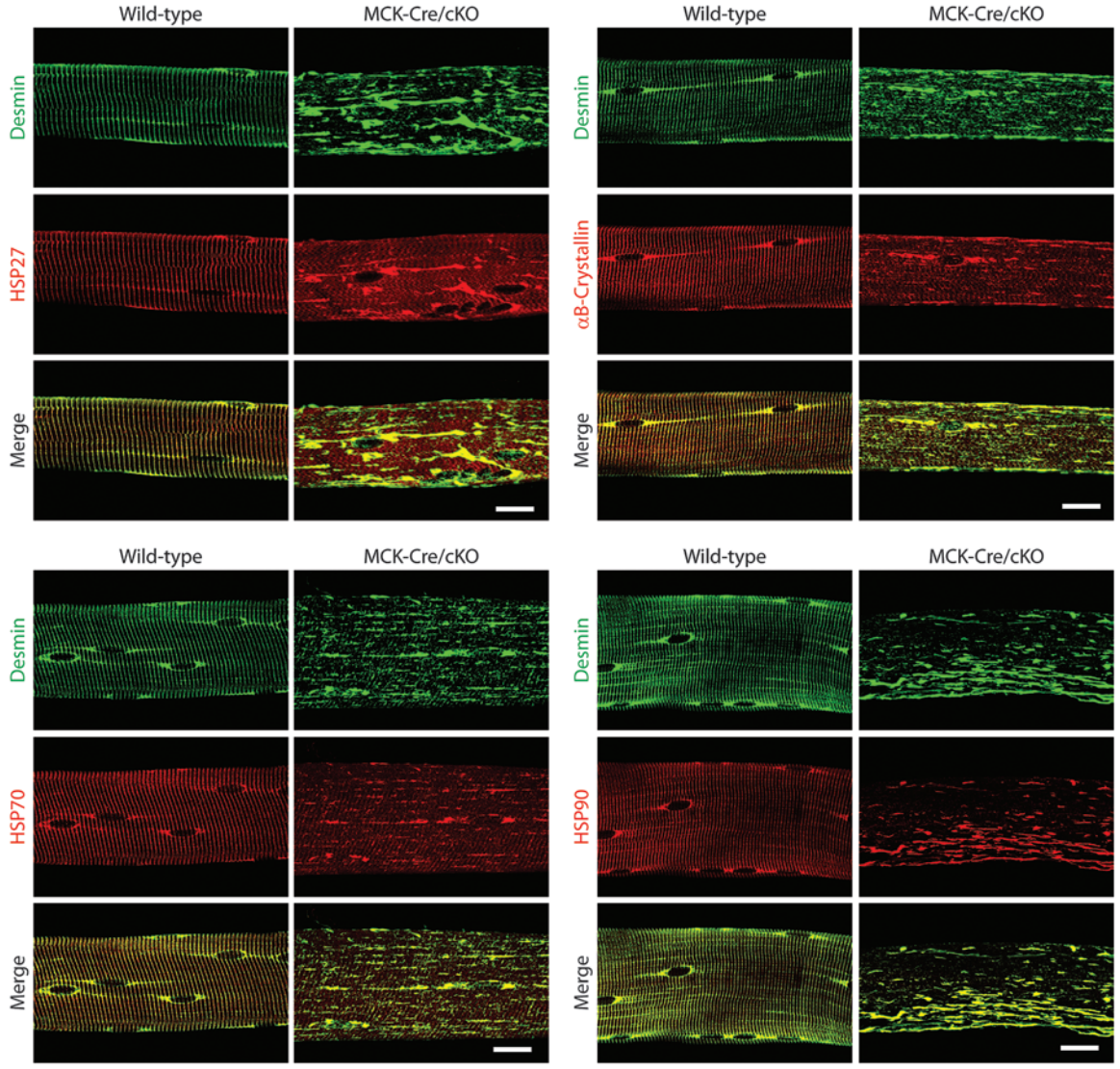

Figure 6
Accumulation of chaperones in desmin-positive protein aggregates in *Plec*$^{-/-}$ muscle fibers. Immunolocalization of HSPs on teased EDL fibers from 3-month-old wild-type and MCK-Cre/cKO mice. Note colocalization of all 4 chaperones tested with desmin-positive IF aggregates in plectin-deficient fibers. Scale bars: 20 μm.

from these data was that at advanced stages of myotube differentiation plectin deficiency led to a marked decrease in the stability of IF networks and sarcomeric structures.

Upregulation of chaperones in plectin-deficient myofibers. Molecular chaperones, including HSPs, assist in the establishment of proper protein conformation and prevent aggregation of partially denaturated proteins (12). HSPs, such as HSP27 (also known as HSP β1, HSPB1) and αB-crystallin (HSPB5), were found to be highly enriched in various myopathies (13).

When the expression levels of various HSPs (HSP27, αB-crystallin, HSP70/HSPA, HSP90/HSPC, mitochondrial HSP60) were analyzed in lysates prepared from plectin-deficient muscle, several chaperones were found to be strongly upregulated (Figure 5A). The overall protein levels of HSP27 and αB-crystallin were found to be increased to 394% and 463%, respectively, compared with wild-type levels. Similarly, HSP70 and HSP90, which are constitutively expressed under normal conditions to maintain protein homeostasis and become actively induced upon environmental stress, showed an increase in their protein levels to 360% and 145%, respectively, of wild-type levels (Figure 5B). In contrast, mitochondrial HSP60 expression levels were decreased to 73% of wild-type levels, reflecting the reduced amount of mitochondria characteristic of plectin-deficient muscle (8).

To monitor chaperone expression during myoblast differentiation, lysates prepared from undifferentiated (day 0) and differentiated cells (days 5, 10, and 15) were analyzed in a similar way (Figure 5C). In this case, the expression of HSP27, αB-crystallin, and HSP70 was found to be induced upon differentiation of myotubes, albeit to various degrees. Compared with those in *Plec*$^{+/+}$ cells, highly increased HSP27 protein levels were detected in *Plec*$^{-/-}$

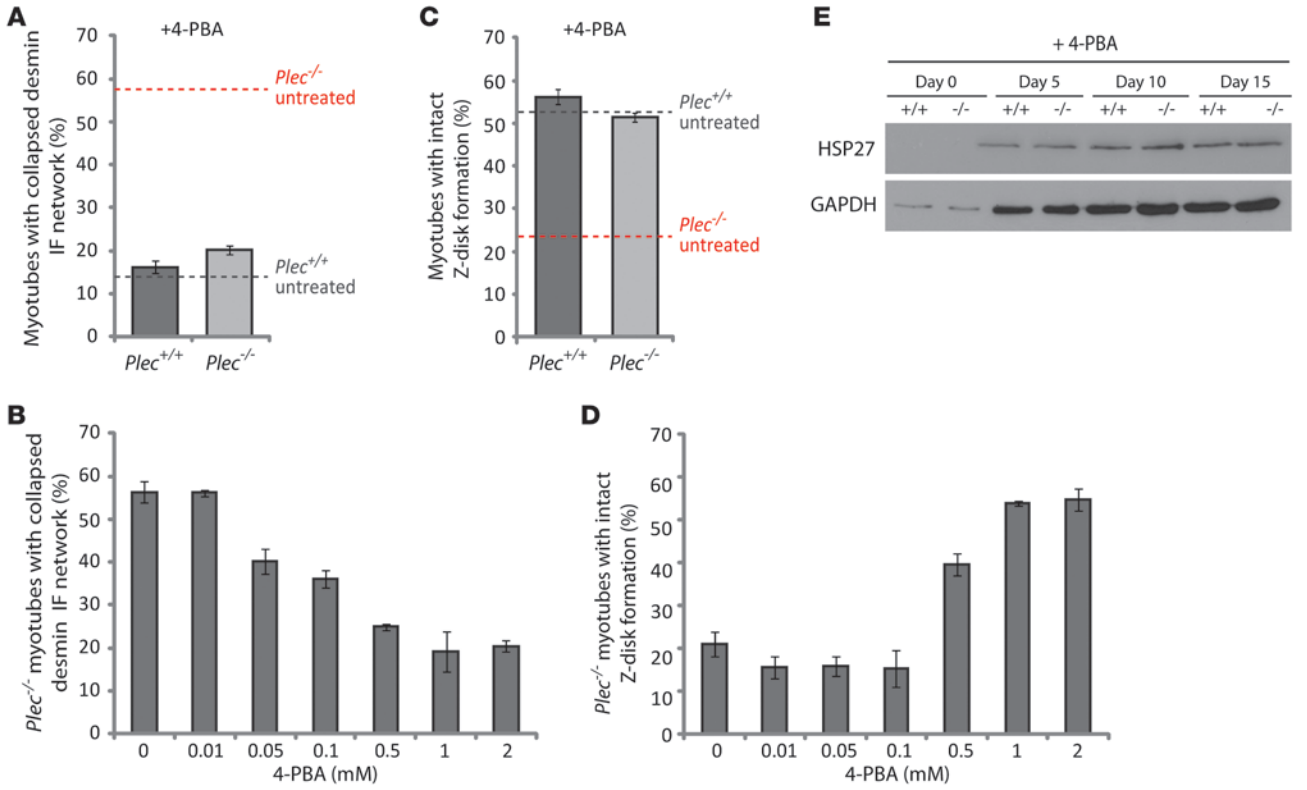

Figure 7

Treatment of differentiated *Plec*$^{+/+}$ and *Plec*$^{-/-}$ myotubes with the chemical chaperone 4-PBA. (**A**) 4-PBA–treated (1 mM) *Plec*$^{+/+}$ and *Plec*$^{-/-}$ myotubes (differentiated for 10 days) were scored for cells with aggregated IFs. Mean ± SEM, 3 experiments (*Plec*$^{+/+}$, $n = 358$; *Plec*$^{-/-}$, $n = 376$). Note drastic reduction of affected myotubes in *Plec*$^{-/-}$ cells compared with untreated cells (dashed lines). (**B**) Dose response block diagram displaying the statistical evaluation of desmin protein aggregate formation in *Plec*$^{-/-}$ myotubes differentiated for 10 days in the presence of increasing concentrations of 4-PBA. (**C**) Z-disk formation in *Plec*$^{+/+}$ and *Plec*$^{-/-}$ myotubes differentiated as in **A**. Mean ± SEM, 3 experiments (*Plec*$^{+/+}$, $n = 357$; *Plec*$^{-/-}$, $n = 438$). Note marked stabilization of sarcomeres in *Plec*$^{-/-}$ myotubes compared to untreated cells (dashed lines). (**D**) Dose response block diagram showing the statistical evaluation of *Plec*$^{-/-}$ cells with intact Z-disk formation after differentiation for 10 days in the presence of increasing concentrations of 4-PBA. Data in **B** and **D** represent mean ± SEM, 3 experiments. (**E**) Immunoblotting of cell lysates from 4-PBA–treated *Plec*$^{+/+}$ and *Plec*$^{-/-}$ myotubes using antibodies to proteins indicated.

lysates. Similarly, a tendency for increased αB-crystallin expression was observed in *Plec*$^{-/-}$ myotubes during differentiation, albeit the difference to *Plec*$^{+/+}$ cells was not statistically significant in this case. The most dramatic increase occurred with HSP27, whose level was more than twice as high in *Plec*$^{-/-}$ myotubes compared to that in *Plec*$^{+/+}$ myotubes after only 5 days of differentiation, reaching a peak around day 10 (Figure 5D).

When plectin-deficient teased EDL fibers were analyzed using immunohistochemistry to assess the subcellular localization of HSPs, colocalization of HSP27, αB-crystallin, HSP70, and HSP90 with desmin-positive protein aggregates was revealed in all cases, whereas wild-type fibers displayed striated staining patterns (Figure 6). Colocalization of these proteins with desmin-containing protein aggregates was also found when frozen sections of plectin-deficient muscle tissue were assessed (Supplemental Figure 4). In contrast, a colocalization of HSPs with desmin aggregates present in *Plec*$^{-/-}$ myotubes could not be observed (L. Winter, unpublished observations).

HSP27 (along with αB-crystallin) has been reported to interact with cellular IFs of the vimentin, keratin, and glial fibrillary acidic protein type as well as with their soluble subunit proteins (14). To investigate whether a similar situation prevailed in differentiated myotubes, we immunoprecipitated desmin from *Plec*$^{+/+}$ and *Plec*$^{-/-}$ myotube cell lysates and analyzed interacting proteins by immunoblotting. As shown in Supplemental Figure 5, HSP27 was coimmunoprecipitated with desmin from both sources, indicating that the interaction between desmin and HSP27 was plectin independent. As expected, the immunocomplexes isolated from *Plec*$^{+/+}$ myotube cell lysates also contained plectin, verifying that plectin, desmin, and HSP27 formed a triple complex (Supplemental Figure 5). Interestingly, the amount of soluble desmin immunoprecipitated from *Plec*$^{-/-}$ myotubes was higher than that of their *Plec*$^{+/+}$ counterparts, consistent with the data obtained by FRAP analysis (compare to Figure 4C).

Phenotype amelioration through chemical chaperone 4-PBA treatment demonstrated in ex vivo myotubes. We hypothesized that *Plec*$^{-/-}$ myotubes, mimicking the hallmarks of plectin-related MFM, could be an ideal tool for screening potential treatment options for patients suffering from plectinopathies. As low-molecular-weight chemical chaperones, similar to HSPs, have the capability to prevent protein aggregation and contribute to the rescue of in vivo aggregated proteins (15), we assessed the effects of 2 of such substances, 4-PBA and

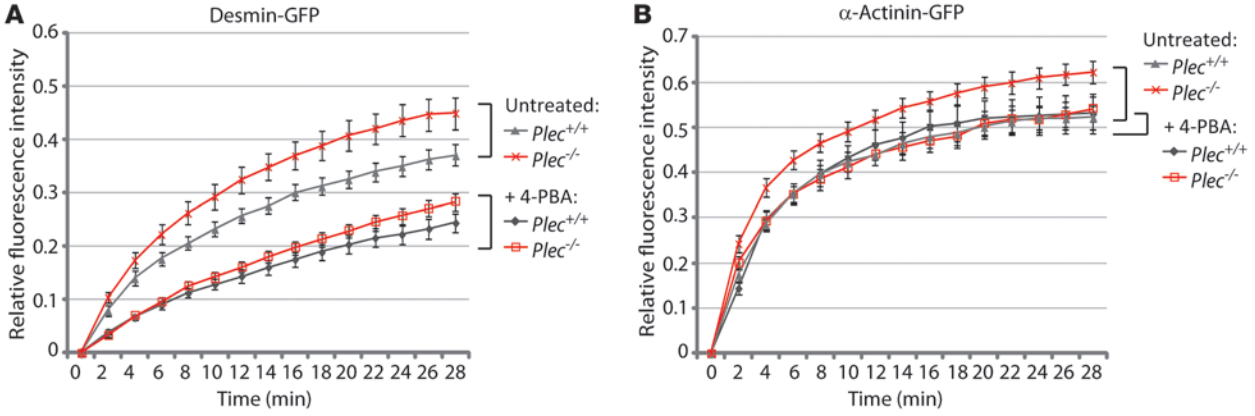

Figure 8

4-PBA treatment of differentiated *Plec*$^{-/-}$ myotubes stabilizes desmin and α-actinin dynamics. (**A**) FRAP analyses of desmin-GFP in *Plec*$^{+/+}$ and *Plec*$^{-/-}$ myotubes differentiated for 10 days with and without 1 mM 4-PBA. Mean ± SEM, 2 experiments (untreated: *Plec*$^{+/+}$, *n* = 54 analyzed ROIs; *Plec*$^{-/-}$, *n* = 55 analyzed ROIs; 4-PBA–treated: *Plec*$^{+/+}$, *n* = 29 analyzed ROIs; *Plec*$^{-/-}$, *n* = 31 analyzed ROIs). (**B**) FRAP analysis of α-actinin–GFP under conditions similar to those in **A**. Mean ± SEM, 2 experiments (untreated: *Plec*$^{+/+}$, *n* = 38 analyzed ROIs; *Plec*$^{-/-}$, *n* = 45 analyzed ROIs; 4-PBA–treated: *Plec*$^{+/+}$, *n* = 21 analyzed ROIs; *Plec*$^{-/-}$, *n* = 30 analyzed ROIs).

trimethylamine N-oxide (TMAO), on aggregate formation in differentiated myotubes. Both of them had been reported to protect EBS keratinocytes from heat stress-induced keratin aggregation (16).

When *Plec*$^{-/-}$ myotubes were differentiated for 10 days in the presence of 1 mM 4-PBA, we could identify desmin-positive aggregates in only 20% of the myotubes examined (Figure 7A), compared with 57% in the case of untreated cells (Figure 2B). This nearly 3-fold reduction clearly indicated a beneficial effect of this chemical, whereas no such effect was revealed when cells were differentiated in the presence of up to 100 mM TMAO (L. Winter, unpublished observation). As shown in a control experiment, the effect of 4-PBA was dependent on the amount administered (Figure 7B). 4-PBA clearly exerted also a stabilizing effect on sarcomere structure, increasing the proportion of myotubes with α-actinin–positive cross-striations from 24% (untreated cells, see Figure 3B) to 51% (Figure 7C), again in a dose-dependent manner (Figure 7D). These observations not only support the notion that immortalized *Plec*$^{-/-}$ myoblasts provide a useful tool for drug screening, but also establish 4-PBA as a first promising candidate for alleviating the symptoms of patients with EBS-MD.

The increase in HSP27 levels observed in *Plec*$^{-/-}$ myotubes during differentiation (Figure 5, C and D) was likely occurring as a cellular reaction to aggregating desmin filaments. In fact, aggregate formation and HSP27 expression both reached their peaks at around the same time (10 days) of differentiation (see Figure 2B and Figure 5D). To examine whether the treatment of cells with 4-PBA had any effect on the expression levels of this protein, *Plec*$^{+/+}$ and *Plec*$^{-/-}$ lysates (from cells differentiated for 0, 5, 10, or 15 days in the presence of 1 mM 4-PBA) were analyzed by immunoblotting. In this case, no obvious differences in total protein levels of HSP27 were observed (Figure 7E), probably because in the presence of 4-PBA, aggregated protein levels were not high enough to trigger expression of the protein.

To study the mechanism behind 4-PBA's ameliorating effect on IF aggregation and sarcomere destabilization, we monitored, using FRAP analyses, the molecular dynamics of desmin and α-actinin in myotubes that had been differentiated in the presence of the compound for 10 days. Interestingly, in both *Plec*$^{+/+}$ and *Plec*$^{-/-}$ myotubes expressing desmin-EGFP, the amount of mobile desmin molecules was found to be decreased compared with that in untreated cells (Figure 8A). In fact, the fluorescence of desmin in photobleached *Plec*$^{+/+}$ myotubes recovered within 28 minutes to only 24% of its initial intensity, compared with 37% in untreated cells. Similarly, in *Plec*$^{-/-}$ myotubes, the recovery rates decreased from 45% in untreated cells to 28% in 4-PBA–treated fibers. Contrary to untreated cells, after 4-PBA treatment, no significant differences between *Plec*$^{+/+}$ and *Plec*$^{-/-}$ cells were revealed, indicating a stabilizing effect of the compound on the IF cytoarchitecture (Figure 8A). Similarly, when recovery rates of α-actinin were analyzed in 4-PBA–treated *Plec*$^{-/-}$ myotubes, the reduced levels of 54% (from 62%) closely resembled the rates observed in *Plec*$^{+/+}$ myotubes (Figure 8B). Thus, in the absence of plectin, the treatment with 4-PBA led to a considerable increase in the rigidity of both the extrasarcomeric desmin IF network and sarcomeric structures.

Finally, to assess whether 4-PBA could improve the resilience of *Plec*$^{-/-}$ myotubes against mechanical strain, we exposed cells spread on flexible membranes to cyclic stretch and assessed their vulnerability by microscopically monitoring their substrate detachment rates (17, 18). In this experiment, 51% of differentiated *Plec*$^{-/-}$ myotubes detached, compared with only 15% of their *Plec*$^{+/+}$ counterparts. In the presence of 4-PBA, the percentage of detached *Plec*$^{-/-}$ myotubes markedly decreased, reaching an intermediate level of 31% (Supplemental Figure 6), supporting the hypothesis that a reduction of the protein aggregate load in *Plec*$^{-/-}$ myotubes leads to an improvement of cellular functions.

Reduction of desmin aggregate formation in muscles of 4-PBA–treated plectin-deficient mice. Given the rescue potential of 4-PBA for desmin aggregate formation in differentiating *Plec*$^{-/-}$ myotubes, we assessed whether a similar effect could be achieved in plectin-deficient mice. For this, we applied a treatment scheme in which wild-type and MCK-Cre/cKO mice were i.p. injected with 200 mg/kg body weight of 4-PBA (or vehicle) for 10 days and sacrificed 24 hours after the final injection. The analysis of skeletal muscle cryosections of wild-type mice showed that desmin IFs were typically located underneath the sarcolemma and at the level of Z-disks, regardless of whether the animals were treated with 4-PBA

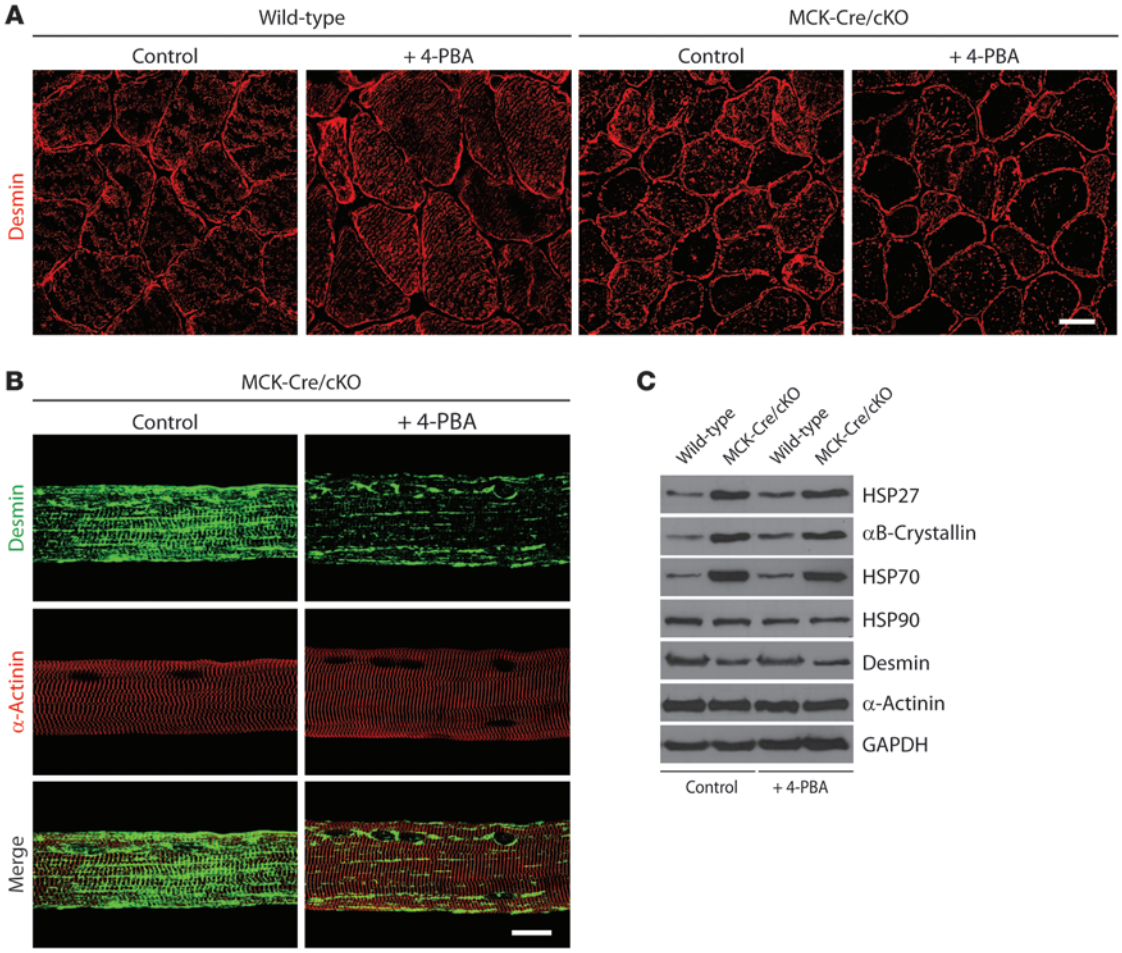

Figure 9

4-PBA treatment ameliorates aggregate formation in plectin-deficient mice. (**A**) Wild-type and MCK-Cre/cKO mice were injected with 4-PBA or vehicle (control) for 10 days. Cryosections of soleus muscles immunolabeled using anti-desmin antibodies are shown. Note reduced formation of desmin aggregates in plectin-deficient muscle after 4-PBA treatment. Scale bar: 20 μm. (**B**) Teased EDL fibers from MCK-Cre/cKO mice (with or without 4-PBA) were coimmunolabeled for α-actinin and desmin. Scale bar: 20 μm. (**C**) Immunoblotting of gastrocnemius muscle lysates obtained from mice (with or without 4-PBA).

(Figure 9A). However, in plectin-deficient muscle (Figure 9A), the situation was different. In untreated (control) mice, massive aggregates of desmin filaments were found in subsarcolemmal regions and throughout the sarcoplasm, regardless of the muscle fiber type (ref. 8 and L. Winter, unpublished data). Strikingly, in muscles from 4-PBA–treated mice, the amount of desmin-positive aggregates in the sarcoplasm appeared to be substantially reduced. Moreover, the signal intensity of subsarcolemmal desmin seemed to be considerably diminished compared with that in control muscle (Figure 9A). Similarly, when teased EDL fibers from control or 4-PBA–treated MCK-Cre/cKO mice were analyzed, the signal intensity of desmin-positive protein aggregates seemed to be markedly reduced upon 4-PBA treatment (Figure 9B). Other phenotypes, such as the disorganization of myofibrillar structures, in particular the misalignment of α-actinin–positive Z-disks, typical of plectin-deficient fibers, showed no improvement upon 4-PBA treatment (Figure 9B). Furthermore, when muscle sections were stained with H&E, the number of centrally nucleated fibers, representing regenerating and immature fibers, was not altered in samples of untreated and 4-PBA–treated MCK-Cre/cKO mice (Supplemental Figure 7, A and B); neither could changes in mitochondrial morphology be observed when tissue sections of control and 4-PBA–treated animals were stained for succinate dehydrogenase (Supplemental Figure 7C).

When the expression levels of HSPs, α-actinin, and desmin were assessed by immunoblotting of skeletal muscle lysates obtained from mice that had been injected with 4-PBA, neither in wild-type nor in MCK-Cre/cKO samples were alterations observed compared to control (noninjected) mice. The higher and lower expression levels of HSPs and desmin, respectively, compared with wild-type muscle were independent of whether 4-PBA was applied or not (Figure 9C).

To obtain quantitative estimates for the reduction of desmin-positive aggregates in myofibers upon 4-PBA application, cross sections of cryosectioned myofibers, immunolabeled for desmin, were analyzed using ImageJ software. To distinguish between signals in subsarcolemmal versus cytoplasmic regions, outer and inner perimeters of desmin-positive ring-like areas underneath the sarcolemma were outlined, as shown in Figure 10A, and the mean intensities of

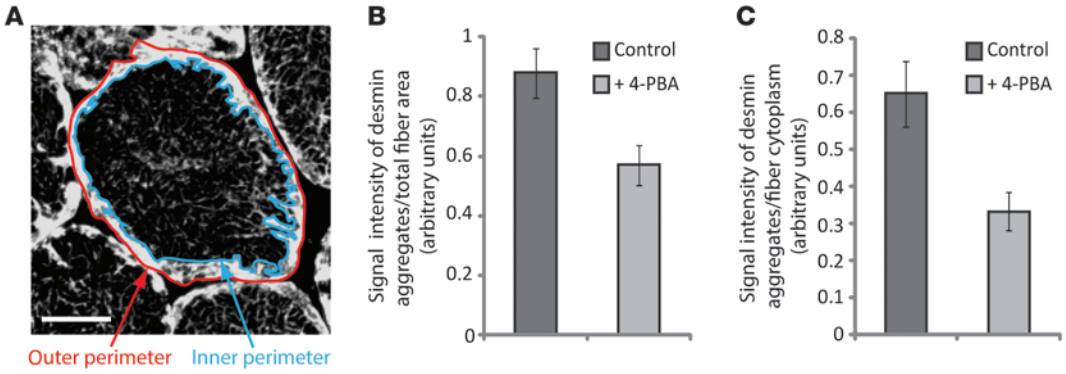

Figure 10

Distribution of desmin aggregates in myofibers from 4-PBA–treated or untreated MCK-Cre/cKO mice. (**A**) Aggregates visualized on cryosections were quantified per individual fiber, or within cytoplasmic subcompartments (containing small desmin aggregates), by outlining the outer (red) and inner (blue) perimeters of the ring-like desmin-positive area underneath the sarcolemma and measuring areas and signal intensities. Scale bar: 10 μm. (**B** and **C**) Statistical evaluations of signal intensities measured in (**B**) total fibers and (**C**) cytoplasmic subcompartments and normalized to total area ($P < 0.01$ and $P < 0.01$, respectively). Note reduced aggregate formation upon 4-PBA treatment. Fibers from untreated ($n = 104$) and 4-PBA–treated ($n = 97$) mice were analyze in 4 independent experiments. Mean ± SEM. Three randomly chosen microscopic fields were analyzed per muscle per experiment ($n = 4$). Statistical significance was determined using an unpaired Student's *t* test.

desmin-specific signals were determined in the two resulting cell compartments. The statistical evaluation of desmin-positive protein aggregates visualized per total cross-sectional area revealed a reduction of signal intensities to 65% of the value estimated for MCK-Cre/cKO mice upon 4-PBA application (Figure 10B). Considering the cytoplasmic area, in which desmin aggregates appear to be smaller than those underneath the sarcolemma, a dramatic drop to 51% of control levels was observed (Figure 10C). Thus, using the chemical chaperone 4-PBA, we achieved a remarkable amelioration of the protein aggregation phenotype characteristic of plectin-related MFM cell and animal models.

In vivo 4-PBA treatment leads to functional muscle improvement in plectin-deficient mice. To test whether in vivo treatment with 4-PBA leads to improved muscle function, two experimental approaches to measure muscle strength in vivo were used. Using a grip strength meter, measurements of forelimb muscle grip strength (Figure 11A), or of total muscle grip strength (forelimbs and hind limbs; Figure 11B), revealed a dramatic decrease in the muscle strength of plectin-deficient mice to 65% and 69% of the respective wild-type levels. When wild-type and MCK-Cre/cKO mice were injected with 4-PBA, already after 10 days of daily injections, a tendency toward improved forelimb grip strength (81% of wild-type level; Figure 11A) and a significant increase in the total grip strength were observed (90% of wild-type level; Figure 11B). After 20 days, the forelimb grip strength of plectin-deficient mice was comparable to that of wild-type animals (Figure 11A). As an alternative, more challenging test for the animals, muscle grip strength was assessed using an inverted mesh grid. In this case, plectin-deficient mice lost their hold and dropped off after 13 seconds, whereas wild-type mice were able to hold on for more than 60 seconds (Figure 11C). Upon 10 and 20 days of 4-PBA treatment, the wire mesh hang time of MCK-Cre/cKO animals on the grid increased to 21 and 24 seconds, respectively (Figure 11C). These data showed that, besides ameliorating the protein aggregate pathology of plectin-related MFM cell and animal models, 4-PBA treatment led to a substantial improvement of skeletal muscle function, setting a first basis for future therapeutic approaches.

Discussion

Further progress in our understanding of human protein aggregate diseases is generally hampered by the fact that diagnostic biopsies from affected patients often reflect late stages of the disease process and are available only in small amounts. Therefore, it is mandatory to establish physiological cell and animal models, which reflect the human pathology and allow analyses of early and intermediate disease stages and the evaluation of novel treatment concepts.

MFM disease-mimicking *Plec*$^{-/-}$ myoblasts display a drastic pathology of their extrasarcomeric as well as sarcomeric cytoskeleton, including protein aggregation. Although immortalized *Plec*$^{-/-}$ myoblasts have the capacity to differentiate from proliferating cells to mature, spontaneously contracting myotubes, they display a diminished survival potential compared with *Plec*$^{+/+}$ controls. This may be attributed to drastic alterations of their IF network architecture, the presence of desmin-positive protein aggregates, and a consecutive disarrangement of the myofibrillar apparatus. Through forced expression of full-length P1d, the isoform responsible for desmin IF network attachment to Z-disks, the observed pathology could be fully reversed. In contrast, the expression of other isoforms typical of skeletal muscle, such as P1, P1b, or P1f, showed no such effect, indicating that the striking desmin filament pathology in EBS-MD muscle tissue is primarily due to a loss of function of isoform P1d, which is most prominently, if not exclusively, expressed in muscle tissue where it is associated with Z-disk structures. Mutations in human desmin have been shown to compromise the assembly and maintenance of IF filaments on various levels (for a review see ref. 19). The loss of plectin, however, exerts its primary deleterious effects by affecting IF network organization in a more general way. Since in *Plec*$^{-/-}$ myoblasts, desmin appears to normally assemble into filaments, plectin seems not to be required for IF network formation per se but has an essential role in the proper attachment of IFs to the myofibrillar apparatus and to other structures, such as the subsarcolemmal and nuclear cytoskeleton, and mitochondria. The faulty attachment and anchorage of IFs in EBS-MD muscle tissue inflicts among other things a misalignment of neighboring myofibrils, probably

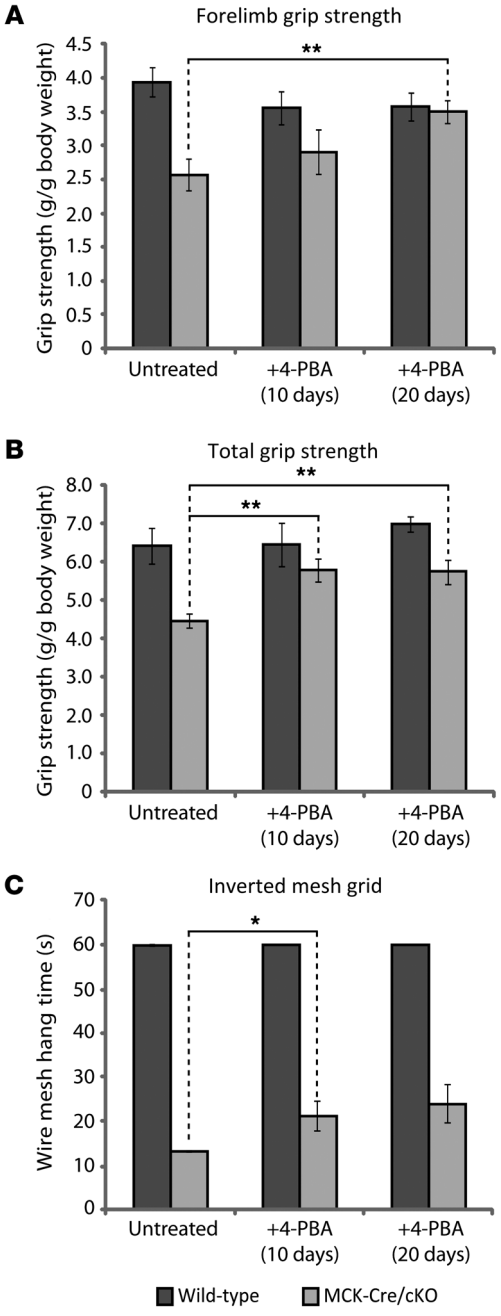

Figure 11

4-PBA treatment increases muscle grip strength of plectin-deficient mice. (**A**) Forelimb grip strength or (**B**) total grip strength (forelimbs and hind limbs) of wild-type and MCK-Cre/cKO mice was assessed before, after 10 days, and after 20 days of i.p. 4-PBA treatment using a grip strength meter. Mean ± SEM (wild-type, $n = 7$; MCK-Cre/cKO, $n = 5$). (**C**) Muscle grip strength was evaluated by measuring the hang time on an inverted wire mesh grid. Mean ± SEM (wild-type, $n = 6$; MCK-Cre/cKO, $n = 5$). $^*P < 0.05$, $^{**}P < 0.01$, paired Student's t test.

leading to their decreased stress resistance and higher mechanical vulnerability. Along with the presence of pathological protein aggregates and mitochondrial dysfunction, these alterations seem to be the key to the molecular pathogenesis of plectin-related EBS-MD muscle pathology.

The molecular mechanism(s) of protein (desmin) aggregate formation in plectin-deficient myofibers and, in particular the question, whether there is a direct connection between this phenomenon and the observed increases in molecular mobility as well as solubility of desmin remain to be solved. Together with observations made in studies on several different cell systems (for details see Supplemental Information), the present study confirms not only plectin's crucial role as IF network organizer in general, but also supports our concept that IFs that are not anchored via plectin at subcellular docking sites become destabilized, more mobile, and presumably more accessible to posttranslational modifications, which in turn might make them more prone to aggregation. Such a mechanism would explain previous results showing that hyperphosphorylation- and oxidative stress–induced (nitrosylation-induced) disruption and collapse of IF networks in plectin-deficient keratinocyte and endothelial cells, respectively, occurred more readily in plectin-deficient cells compared with wild-type cells (20, 21). The fact that plectin deficiency concurred with spontaneous protein aggregate formation in myotubes, but not in the other previously tested cell systems, probably reflects the higher mechanical load of these cells due to their spontaneous contraction.

The small HSP HSP27 has been reported to interact with IFs of the vimentin, keratin 18, and glial fibrillary acidic protein type even without heat shock, and it has been suggested to play a role in filament assembly and the control of interfilament interactions (14). The pull-down of HSP27 with desmin from myoblast cell lysates confirms this notion and extends its potential relevance to the muscle cell system. As plectin was also found to be part of the precipitated immunocomplexes, one might anticipate a stabilizing and orchestrating function of plectin for HSP27-desmin IF complexes during myotube formation. In this context, the increased expression of chaperones, as observed in plectin-deficient muscle, presumably is a reaction of the cell to facilitate folding of damaged proteins or degradation of aggregated proteins. Similar to what we observed for plectin-related MFM, a predominant localization of chaperones (and of other proteins involved in protein degradation pathways) within protein aggregates has been described for other MFMs, such as filaminopathies (22), myotilinopathies, and desminopathies (23). Most strikingly, highly increased protein levels of HSP27 as well as a tendency for increased αB-crystallin became apparent even during differentiation of plectin-deficient myotubes, indicating that chaperones represented the first line of defense against desmin network aggregation. This is in line with other studies showing that IFs interact with HSPs like HSP70 and HSP90 and especially the small HSPs, HSP27 and αB-crystallin, under conditions of stress (24). Our results demonstrate that, in the case of MFM-mimicking myotubes, protein control mechanisms and chaperone expression are activated but do not secure the cell against protein aggregate formation.

To date, no specific or ameliorating pharmacological therapy is available for plectin-related MFM and other genetic forms of MFMs. In general, HSPs function as molecular chaperones, preventing stress-induced protein aggregation of partially denaturated proteins by stabilizing proteins against misfolding or removing them when misfolded (25). As the massive overexpression of individual chaperones observed in plectin-deficient muscle fibers evidently was insufficient to prevent protein aggregation, we used our newly established MFM cell model to investigate

whether a substance, such as the chemical chaperone 4-PBA, might have an ameliorating effect on the phenotype. Reduced formation of desmin-positive protein aggregates and increased sarcomere stability in plectin-deficient myotubes, as observed by immunofluorescence microscopy and FRAP analyses, indeed indicated a beneficial and cell protective effect of this compound in a dose-dependent manner. Evidently, 4-PBA cannot restore plectin-mediated desmin IF anchorage, but it probably stabilizes the filament networks within the myofiber and reduces misfolding by increasing protein solubility. Similar phenotype-ameliorating effects have been reported for mutant (G165fsX8) γD-crystallin, for which 4-PBA treatment enhanced the solubility of the mutant protein (26), and for a rotenone-induced mouse model of Parkinson's disease, for which 4-PBA treatment was shown to decrease the protein level of α-synuclein (27).

By monitoring a reduction in desmin aggregate formation in myofibers upon 4-PBA treatment of plectin-deficient mice, we demonstrated that immortalized MFM myoblasts represent a reliable tool for drug screening and thus provide a basis for the future development of therapeutic strategies. After just a relatively short 10-day 4-PBA administration period, we achieved a marked reduction of the desmin aggregate load in plectin-deficient mice. Other features characteristic of human patients suffering from plectinopathies and MCK-Cre/cKO mice, such as increased amounts of centrally nucleated fibers or mitochondrial accumulations (8), were not changed during this time, albeit one may anticipate amelioration of additional pathologic alterations with prolonged administration of the compound. Most strikingly, however, a treatment with 4-PBA for 10 days significantly increased muscle functionality of plectin-deficient mice, as reflected by their increased grip strength. This functional improvement was further increased by prolonging the administration of 4-PBA to 20 days, consistent with a time-dependent effectiveness of the treatment.

Our study adds EBS-MD to a list of diseases that are improvable by treatment with 4-PBA. This compound has been shown to reduce protein mislocalization in diseases such as cystic fibrosis, cerebral ischemic injury, diabetes, Alzheimer's disease, and familial Parkinson's disease (28–32), and it has been approved for clinical use in patients with cystic fibrosis and to treat urea cycle disorders (28, 33). Our results have potential clinical relevance, as they point out a pathological mechanism of desmin protein aggregation effected by plectin deficiency. MFM cell and animals models, like the ones we have described here, could be useful for large-scale screening and testing of pharmacological compounds, laying the basis for future therapeutic approaches.

Methods

Cell culture. Skeletal myoblasts were isolated according to a protocol modified from refs. 34 and 35 using the limbs of neonatal *Plec*$^{-/-}$ (9) and wild-type littermate mice. For the isolation of immortalized cell lines, corresponding mouse lines crossed into a *p53*$^{-/-}$ background were used (11). Details of myoblast isolation, cultivation, and treatment are described in the Supplemental Methods.

Mouse model and treatment. Twelve-week-old wild-type mice homozygous for the floxed plectin allele (*Plec*$^{fl/fl}$) or conditional (MCK-Cre) striated muscle-restricted plectin knockout mice (cKO; ref. 8), both in a C57BL/6 background, were treated once daily with 4-PBA (200 mg/kg, i.p.) or vehicle for 10 days. Details for muscle strength assessments are provided in the Supplemental Methods.

Supplemental Methods. A list of antibodies used in this work as well as a description of immunofluorescence microscopy and histology, preparation of cell and tissue lysates, FRAP analysis, coimmunoprecipitation, and cell stretcher experiments are provided in detail in the Supplemental Methods.

Statistics. Comparison between the values of 2 groups was performed using an unpaired, 2-tailed Student's *t* test. For statistical analyses of muscle grip strength measurements, a paired, 2-tailed Student's *t* test was used. A *P* value of less than 0.05 was considered statistically significant.

Study approval. Animal studies were approved by the Federal Ministry for Science and Research (BMWF), Vienna, Austria.

Acknowledgments

We thank Mumna Al Banchaabouchi (core preclinical phenotyping facility, VBC Vienna) for introducing us to grip strength measurements and help in data interpretation and Maggie C. Walter (Ludwig-Maximilians-University Munich, Germany) and Dieter O. Fürst (University of Bonn, Germany) for providing expression plasmids. This work was supported by Austrian Science Research Fund (FWF) grants P23729-B11 and I413-B09 (part of the Multilocation DFG-Research Unit 1228 "Molecular Pathogenesis of Myofibrillar Myopathies") and doctoral program grant W1220; travel support was provided by NanoNet COST Action (BM 1002).

Received for publication July 2, 2013, and accepted in revised form November 21, 2013.

Address correspondence to: Gerhard Wiche, Department of Biochemistry and Cell Biology, Max F. Perutz Laboratories, University of Vienna, Dr. Bohrgasse 9, 1030 Vienna, Austria. Phone: 43.1.4277.52852; Fax: 43.1.4277.9748; E-mail: gerhard.wiche@univie.ac.at.

Lilli Winter's present address is: Institute of Neuropathology, University Hospital Erlangen, Erlangen, Germany.

1. Ferrer I, Olive M. Molecular pathology of myofibrillar myopathies. *Expert Rev Mol Med*. 2008;10:e25.
2. Schröder R, Schoser B. Myofibrillar myopathies: a clinical and myopathological guide. *Brain Pathol*. 2009;19(3):483–492.
3. Winter L, Wiche G. The many faces of plectin and plectinopathies: pathology and mechanisms. *Acta Neuropathol*. 2013;125(1):77–93.
4. Wiche G, Winter L. Plectin isoforms as organizers of intermediate filament cytoarchitecture. *Bioarchitecture*. 2011;1(1):14–20.
5. Castañón MJ, Walko G, Winter L, Wiche G. Plectin-intermediate filament partnership in skin, skeletal muscle, and peripheral nerve. *Histochem Cell Biol*. 2013;140(1):33–53.
6. Fuchs P, et al. Unusual 5′ transcript complexity of plectin isoforms: novel tissue-specific exons modulate actin binding activity. *Hum Mol Genet*. 1999; 8(13):2461–2472.
7. Rezniczek GA, et al. Plectin 1f scaffolding at the sarcolemma of dystrophic (mdx) muscle fibers through multiple interactions with beta-dystroglycan. *J Cell Biol*. 2007;176(7):965–977.
8. Konieczny P, et al. Myofiber integrity depends on desmin network targeting to Z-disks and costameres via distinct plectin isoforms. *J Cell Biol*. 2008; 181(4):667–681.
9. Andrä K, et al. Targeted inactivation of plectin reveals essential function in maintaining the integrity of skin, muscle, and heart cytoarchitecture. *Genes Dev*. 1997;11(23):3143–3156.
10. Becher UM, et al. Enrichment and terminal differentiation of striated muscle progenitors in vitro. *Exp Cell Res*. 2009;315(16):2741–2751.
11. Metz T, Harris AW, Adams JM. Absence of p53 allows direct immortalization of hematopoietic cells by the myc and raf oncogenes. *Cell*. 1995;82(1):29–36.
12. Sun Y, MacRae TH. The small heat shock proteins and their role in human disease. *FEBS J*. 2005; 272(11):2613–2627.
13. Fischer D, Matten J, Reimann J, Bönnemann C, Schröder R. Expression, localization and functional divergence of alphaB-crystallin and heat shock protein 27 in core myopathies and neurogenic atrophy. *Acta Neuropathol*. 2002;104(3):297–304.
14. Perng MD, Cairns L, van den IP, Prescott A, Hutcheson AM, Quinlan RA. Intermediate filament interactions can be altered by HSP27 and alphaB-crystallin. *J Cell Sci*. 1999;112(pt 13):2099–2112.
15. de Marco A. Molecular and chemical chaperones for improving the yields of soluble recombinant pro-

teins. *Methods Mol Biol*. 2011;705:31–51.
16. Chamcheu JC, Navsaria H, Pihl-Lundin I, Liovic M, Vahlquist A, Torma H. Chemical chaperones protect epidermolysis bullosa simplex keratinocytes from heat stress-induced keratin aggregation: involvement of heat shock proteins and MAP kinases. *J Invest Dermatol*. 2011;131(8):1684–1691.
17. Bonakdar N, et al. Biomechanical characterization of a desminopathy in primary human myoblasts. *Biochem Biophys Res Commun*. 2012;419(4):703–707.
18. Soltow QA, Zeanah EH, Lira VA, Criswell DS. Cessation of cyclic stretch induces atrophy of C2C12 myotubes. *Biochem Biophys Res Commun*. 2013; 434(2):316–321.
19. Clemen CS, Herrmann H, Strelkov SV, Schröder R. Desminopathies: pathology and mechanisms. *Acta Neuropathol*. 2013;125(1):47–75.
20. Osmanagic-Myers S, Gregor M, Walko G, Burgstaller G, Reipert S, Wiche G. Plectin-controlled keratin cytoarchitecture affects MAP kinases involved in cellular stress response and migration. *J Cell Biol*. 2006;174(4):557–568.
21. Spurny R, et al. Oxidation and nitrosylation of cysteines proximal to the intermediate filament (IF)-binding site of plectin: effects on structure and vimentin binding and involvement in IF collapse. *J Biol Chem*. 2007;282(11):8175–8187.
22. Kley RA, et al. Pathophysiology of protein aggregation and extended phenotyping in filaminopathy. *Brain*. 2012;135(pt 9):2642–2660.
23. Olivé M. Extralysosomal protein degradation in myofibrillar myopathies. *Brain Pathol*. 2009;19(3):507–515.
24. Wettstein G, Bellaye PS, Micheau O, Bonniaud P. Small heat shock proteins and the cytoskeleton: an essential interplay for cell integrity? *Int J Biochem Cell Biol*. 2012;44(10):1680–1686.
25. Morimoto RI. Proteotoxic stress and inducible chaperone networks in neurodegenerative disease and aging. *Genes Dev*. 2008;22(11):1427–1438.
26. Gong B, Zhang LY, Lam DS, Pang CP, Yam GH. Sodium 4-phenylbutyrate ameliorates the effects of cataract-causing mutant gammaD-crystallin in cultured cells. *Mol Vis*. 2010;16:997–1003.
27. Inden M, et al. Neurodegeneration of mouse nigrostriatal dopaminergic system induced by repeated oral administration of rotenone is prevented by 4-phenylbutyrate, a chemical chaperone. *J Neurochem*. 2007;101(6):1491–1504.
28. Rubenstein RC, Zeitlin PL. A pilot clinical trial of oral sodium 4-phenylbutyrate (Buphenyl) in delta-F508-homozygous cystic fibrosis patients: partial restoration of nasal epithelial CFTR function. *Am J Respir Crit Care Med*. 1998;157(2):484–490.
29. Qi X, Hosoi T, Okuma Y, Kaneko M, Nomura Y. Sodium 4-phenylbutyrate protects against cerebral ischemic injury. *Mol Pharmacol*. 2004;66(4):899–908.
30. Ozcan U, et al. Chemical chaperones reduce ER stress and restore glucose homeostasis in a mouse model of type 2 diabetes. *Science*. 2006;313(5790):1137–1140.
31. Ricobaraza A, Cuadrado-Tejedor M, Perez-Mediavilla A, Frechilla D, Del Rio J, Garcia-Osta A. Phenylbutyrate ameliorates cognitive deficit and reduces tau pathology in an Alzheimer's disease mouse model. *Neuropsychopharmacology*. 2009;34(7):1721–1732.
32. Ono K, et al. A chemical chaperone, sodium 4-phenylbutyric acid, attenuates the pathogenic potency in human alpha-synuclein A30P + A53T transgenic mice. *Parkinsonism Relat Disord*. 2009;15(9):649–654.
33. Lee B, et al. Phase 2 comparison of a novel ammonia scavenging agent with sodium phenylbutyrate in patients with urea cycle disorders: safety, pharmacokinetics and ammonia control. *Mol Genet Metab*. 2010;100(3):221–228.
34. Cerletti M, et al. Highly efficient, functional engraftment of skeletal muscle stem cells in dystrophic muscles. *Cell*. 2008;134(1):37–47.
35. Rando TA, Blau HM. Methods for myoblast transplantation. *Methods Cell Biol*. 1997;52:261–272.